Porous microneedle patch with sustained exosomes delivery repairs severe spinal cord injury

Ao Fang[1,2,3,6], Yifan Wang[1,6], Naiyu Guan[1,2,3,6], Lingmin Lin[1,2], Binjie Guo[1,2,3], Wanxiong Cai[2], Xiangfeng Chen[1,2], Jingjia Ye[1,2], Zeinab Abdelrahman[1,2,3], Shuang Jin[2], Xiaosong Gu[4], Bin Yu[4], Xuhua Wang[1,2,3,5] *

Affiliations:

1. Department of Neurobiology and Department of Orthopedics, 2nd Affiliated Hospital, Zhejiang University School of Medicine, Zhejiang University, Hangzhou, Zhejiang Province, 310003, PR China

2. NHC and CAMS Key Laboratory of Medical Neurobiology, MOE Frontier Science Center for Brain Research and Brain–Machine Integration, School of Brain Science and Brain Medicine, Zhejiang University, Hangzhou, Zhejiang Province, 310003, PR China

3. Department of Rehabilitation Medicine, First Affiliated Hospital, College of Medicine, Zhejiang University, Hangzhou, Zhejiang Province, 310003, PR China

4. Key Laboratory of Neuroregeneration of Jiangsu and Ministry of Education, NMPA Key Laboratory for Research and Evaluation of Tissue Engineering Technology Products, Nantong University, Nantong, China

5. Co-innovation Center of Neuroregeneration, Nantong University, Nantong, 226001 Jiangsu, PR China

6. These authors contributed equally

* Correspondence: xhw@zju.edu.cn (X.W.)

1. Abstract

The transplantation of mesenchymal stem cells-derived exosomes (MSC-EXO) has been suggested as an efficacious treatment to suppress SCI-triggered neuroinflammation. However, an ethically acceptable method to continuously deliver MSC-EXO into the acute spinal lesion without damaging spared tissues/axons has never been achieved. In this study, we fabricated a device that consists of a patch containing MSC and microneedle array (MN-MSC patch) to treat severe SCI. When topically applied to the acute spinal lesion beneath spinal dura, the soft microneedle (MN) array with good mechanical strength avoids damages to the spared spinal tissues and the porous microstructure of MN facilitates highly efficient MSC-EXO delivery. With the capacity to sustainedly deliver MSC-EXO, the MN-MSC patch was evaluated in a contusive rat SCI model and showed that the MSCs encapsulated in the patch could survive for at least 7 days, which covers the optimal time window for down-regulating SCI-triggered neuroinflammation. As a result, the MN-MSC patch treatment leads to reduced cavity and scar tissue formation, angiogenesis, and the survival of spared tissues/axons. Remarkably, the rats treated by this method achieved superior muscle control and exhibited robust hindlimb locomotion functional recovery. Conclusively, the MN-MSC patch device proposed here breaks through the current dilemma from the contradiction between treatment efficacy and ethical issues in treating acute SCI.

Keywords: Spinal cord injury; Microneedle patch; Exosomes; Sustained delivery; Mesenchymal stem cells.

2. Introduction

There are about 930,000 new spinal cord injury (SCI) cases caused by accidents each year.[1] Even though the systemic administration of methylprednisolone sodium succinate (MPSS) has been approved as the only drug for treating acute SCI, this drug is with limited therapeutic efficacy and severe side effects, which severely limited its application in clinical practice.[2] SCI is initially caused by mechanical trauma and diverse mechanisms of secondary damage following the inflammatory response.[3] The secondary damage can cause hemorrhage, edema, decreased blood flow and inflammation, affecting adjacent spinal cord segments.[4] The inflammatory environment triggered by the activation of microglia and releasing pro-inflammatory cytokines leads to inevitable neuronal damage and consequently scar and cystic cavity formation in the spinal lesion sites.[5] Recently, the transplantation of mesenchymal stem cells (MSCs) into the lesion sites has been suggested as an effective treatment to alleviate the neuroinflammation triggered by SCI[6] and promote injury healing.[7] However, the SCI lesion's neuroinflammatory microenvironment is harmful for MSCs survival, significantly impeding their clinical application.[8]

Fortunately, MSC-derived exosomes (MSC-EXO) secreted by MSCs have similar therapeutic benefits for immune modulation when injected into an acute SCI lesion.[9] Previous studies have shown that the transplantation of MSC-EXO immobilized in a peptide-modified adhesive hydrogel into an SCI lesion during the acute phase could mitigate the SCI microenvironment and promote functional recovery.[10] However, the retention time of MSC-EXO in the spinal tissue might not be long enough to exhibit their optimal therapeutic effects. The neuroinflammation and neuronal apoptosis caused by SCI could continue for a couple of weeks or even longer,[11] but MSC-EXO could not be continuously delivered into the lesion of SCI by these methods. Moreover, direct transplantation of MSC-EXO into the spinal injury site might damage spared tissue adjacent to the lesion, cause unpredictable side effects and increase medical accidents.[12] Therefore, in clinical practice, the direct transplantation of MSC-EXO or materials containing MSC-EXO into the spinal lesion of an acute SCI patient is refractory to be ethically approved.[13]

To overcome these challenges, we took the advantages of microneedle (MN) array, which has facilitated painless localized delivery of drugs or therapeutic biomolecules with good toleration in clinical trials.[14] We then fabricated a patch with MN array with good mechanical strength matching soft spinal tissues and suitable pore size for MSC-EXO delivery when it is mounted onto a spinal cord lesion beneath the dura. To sustainedly deliver MSC-EXO, the MN array was additionally mounted with a GelMA hydrogel block embedded with MSCs (MN-MSC patch) during surgery (Scheme 1). We envisioned that the GelMA hydrogel block could provide a biocompatible microenvironment for the long-term survival of

MSCs which can secrete and deliver MSC-EXO to the spinal lesion sustainedly for a long time. In this way, the MSC-EXO can be efficiently and precisely delivered to the SCI lesion without extra damage through the porous MNs for optimal therapeutic efficacy (Scheme 1). We showed that the MN-MSC patch could keep on the spinal injury sites and sustainedly release MSC-EXO for at least one week, which results in remarkable tissue repair, superior muscle control and robust functional recovery after severe SCI (Scheme 1).

3. Results

3.1 Fabrication and Characterization of the Patch with MN array *in vitro*

To avoid injecting MSCs into the spinal cord and causing damages to spared spinal tissue adjacent to the spinal cord lesions, we designed a patch with MN array (MN patch) (Fig. 1a). The MN patch is made from chemically cross-linked methacryloyl (MW. 100-250kDa) to form gelatin methacryloyl (GelMA) with a micromolding method (Fig. 1a, a1, a2)[15] . The scale of the fabricated MN patch is about 4 mm × 4 mm with 45 needles, which is big enough to cover a typical rat contusive spinal cord lesion. The needle of the MN array is conical, with a base diameter of 250 μm, a height of 600 μm and a tip diameter of 10 μm (Fig. 1e-g). To sustainedly release exosomes, the patch was additionally covered with GelMA hydrogel embedded with MSCs during surgery (Supplementary Fig. S2d-g). The GelMA hydrogel with porous structures was designed to facilitate the release of MSC-EXO through the polymeric needles. As shown by the scanning electron microscopy (SEM) images, the pore size of the gel reaches up to about 100 μm (Fig. 1b, b2, b4), compared with the relative smaller pore size of 10 μm in the traditional GelMA hydrogel (Fig. 1b, b1, b3).

To examine the biocompatibility of the MN patch, we first dropped the methacryloyl solution with MSCs (about 2.5×10^7 cells/mL) on the surface of the patch and cross-linked methacryloyl to form GelMA hydrogel with blue light irradiation (Fig. 1a, a3, a4). The live/dead staining of GelMA hydrogel revealed excellent viability of embedded MSCs after culturing for 3 and 5 days (Fig. 1c). Quantitative analysis with CCK8 test indicated that MSCs in GelMA hydrogel of MN-MSC patch survive and proliferate well (Fig. 1d). The mechanical strength of per needle constructed by the porous structure was matching the soft spinal cord tissue.[16] It has a relatively lower mechanical strength than the normal one, which is propitious to avoid damaging the spinal cord (Fig. 1h). We then first assessed the MSC-EXO release capacity of MN patch with this porous structure. To do so, the patch made from porous GelMA or regular GelMA was seeded with MSCs and placed into the top well of a transwell (Fig. 1i). The transwells were then immersed in culture media and incubated at 37 ℃. At regular intervals, aliquots of samples were collected from the bottom wells, and the concentrations of MSC-EXO in the samples were measured by a Micro BCA Protein Assay kit.[17] Plotting the OD value of the samples revealed that the MN patch made from porous GelMA release

MSC-EXO more efficiently (Fig. 1j), possibly because the MN patch with bigger pore size was more permissive for MSC-EXO. We therefore chose the MN patch made from porous GelMA for the following studies.

As we know, most of the therapeutic benefits of MSCs in SCI treatment were through MSC-EXO release,[18] highlighting the importance of sustained MSC-EXO delivery in improving therapeutic efficacy. We therefore sought to evaluate the sustained MSC-EXO delivery capacity of MN patch embedded with MSCs (MN-MSC), and MN patch loaded with MSC-EXO (MN-EXO) was used as control. The MSC-EXO were isolated from the culture supernatant of MSCs via ultracentrifugation and showed a typical cup-shaped morphology (Supplementary Fig. S1a). Through a nanoparticle tracking analysis (NTA), we found that the MSC-EXO is with an average size of 110 nm, consistent with the results of previous studies (Supplementary Fig. S1c).[19] The expression of tetraspanins CD9 and TSG101 (mesenchymal markers) on the collected samples (Supplementary Fig. S1d) indicated successful isolation and purification of MSC-EXO. We then compared the persistent MSC-EXO release capacity of MSCs seeded and MSC-EXO loaded MN-patch. Plotting the relative concertation of released MSC-EXO in the collected samples from the bottom wells of the transwells at different time points revealed that the release of MSC-EXO from MSC-EXO loaded MN-patch quickly deceased in the first 4 days, whereas the delivery of MSC-EXO from MSC seeded MN patch was stable but with slight increase in 2 weeks (Fig. 1k), indicating that the MN patch had good biocompatibility for MSC survival. Thus, we fabricated a device to persistently deliver MSC-EXO with high efficiency.

3.2 Distribution of Exosomes in the Injured Spinal Cord after MN Patch Implantation

After verifying that the fabricated MN-MSC patch could sustainedly deliver exosomes *in vitro*, we sought to assess whether the MSC-EXO of the patch could be delivered through the MN into injured spinal cord tissues in a contusive rat SCI model. We used a severe T10 contusive SCI model, which was constructed by an Infinite Vertical impactor with the parameter of 2.5 m/s rate, 2 mm depth, 5 s duration time and 3 mm diameter cylinder.[20] Because the MSC-EXO in live MSCs are hard to be labelled, the MSC-EXO stained with CM-DiI were encapsulated into GelMA hydrogel in this experiment. The solid red fluorescence of MSC-EXO encapsulated in the GelMA hydrogel indicted successful labeling of them with CM-DiI (Supplementary Fig. S1b). After contusive SCI, the dura of spinal cord was removed carefully by a pair of surgical scissors. And then the MN patch was placed on top of the spinal lesion, and a solution of GelMA mixed with MSC-EXO was mounted onto the top of MN patch

followed by a blue light photocuring process (Fig. 2a). 7 days after surgery, we found that most of the released MSC-EXO were localized and aggregated in the spinal injury site (Fig. 2b and c, b1, b2, c1, c2), indicating the localized delivery capacity of the MN patch. Conclusively, the MN patch has excellent localized delivery capacity of MSC-EXO *in vivo*, which facilitates sustained MSC-EXO delivery for SCI treatment.

Next, we attempted to assess whether the cells in the MN-MSC patch could survive long enough to ameliorate the SCI-induced neuroinflammatory environment and protect spared tissues/axons from secondary injuries. We implanted the MN patch onto the spinal lesion of the same SCI model, and the solution of MSCs mixed with GelMA was mounted onto the top of the MN patch before the blue light photocuring process (Fig. 2a, S2a-h). As we know, the optimal time for suppressing acute SCI-triggered neuroinflammation and protecting spared tissue/axons is within 7 days after SCI,[21] so we dissected the spinal cord on the 7th day after SCI to assess whether MSCs could survive in the MN-MSC patch by this time point. As indicated by the images of spinal sections stained with hematoxylin and eosin (H&E) (Fig. 2d), the MN patch still persists on the spinal cord's surface at this time. More importantly, human MSC marker GAPDH staining of the spinal tissues indicated that the MSCs survived well in the MN-MSC patch at the 7th day after SCI (Fig. 2e, f, red). These results confirmed that the MSCs in the MN-MSC patch can survive at the injury site long enough to cover the optimal therapeutic time window of SCI. Moreover, immunofluorescent staining of a serial spinal section from the spinal border to the center showed that MSCs from the MN-MSC patch did not migrate from the GelMA hydrogel block into the spinal cord (Fig. S3). These results indicated that the fabricated device achieved our aim to sustainedly deliver MSC-EXO without MSCs invading into the spinal cord.

3.3 The MN-MSC Patch Alleviates Inflammatory Response in the Spinal Lesion after SCI

To assess whether the MN-MSC patch could ameliorate the SCI-induced neuroinflammatory environment, we constructed animal models without any treatment (control group), with MN patch embedded with MSC-EXO implantation (MN-EXO group) or MN patch seeded with MSC implantation (MN-MSC group) for comparison. On day 7, we detected protein expression levels of the spinal tissues with spinal lesions of rats with different treatments by western blotting analysis. We found that the expression of the pro-inflammatory MMP-9 marker was significantly reduced and the expression of the anti-inflammatory TGF-β marker was significantly increased in the spinal tissues of rats with the MN-MSC patch treatment (Fig. 2g, h, i). In addition, the expression of the proapoptotic marker BAX was significantly reduced

(Fig. 2g, j), and the angiogenic Arg-2 marker was significantly increased in the spinal tissues of rats with the MN-MSC patch treatments (Fig. 2g, k). In contrast, we found nearly no significant differences in these gene expressions between MN-EXO and control groups (Fig. 2g-k), possibly because the limited number of exosomes delivered by MN-EXO was not enough to significantly suppress the SCI-triggered neuroinflammation. These results indicated that the sustained MSC-EXO delivery was the key to efficiently alleviate the neuroinflammatory microenvironment in the spinal lesion after SCI.[22]

To further analyze the tissue-protective efficacy, sagittal sections of injured spinal cords at 8 weeks post-SCI were analyzed with immunofluorescence staining. As a result, the section images with Iba1 (macrophages/microglia) staining indicated that the activated immune cells in the rats reduced significantly with the MN-MSC patch treatment compared with that of the rats with control or MN-EXO treatment (Supplementary Fig. S4a, e). On the contrary, more neurons (NeuN) (Supplementary Fig. S4b, f), blood vessels (CD31) (Supplementary Fig. S4c, g), myelin (MBP) (Supplementary Fig. S4d, h) and astrocytes (GFAP) (Supplementary Fig. S4a-d, i) were observed in spinal tissues of MN-MSC group. These results further verified that the MN-MSC patch treatment could reduce the SCI-triggered inflammation and protect the neurons, oligodendrocytes, astrocytes and blood vessels from secondary injury after SCI.

3.4 MN-MSC Patch Protects Spared Tissues/axons from Secondary Injury

After verifying that MN-MSC treatment could reduce the SCI-triggered inflammation, we sought to assess whether this treatment could protect spared tissues/axons from secondary Injury after SCI. To determine whether more descending axons could survive in the condition of being treated with an MN-MSC patch, we injected AAV2/9-hSyn-mCherry into T7-T8 of the 3 groups of rats 2 weeks before sacrifice to trace the descending propriospinal axons (Fig. 3a). First of all, we found that the spinal cord shape deformation treated by MN-MSC patch after 8 weeks is significantly less than that of rats in the control and MN-EXO groups (Fig. 3b). After staining the spinal sections with a red fluorescent protein (RFP) antibody (Fig. 3c), we found that the RFP^+ propriospinal axons exhibited no significant difference in coronal sections of spinal segments above the injury site of rats in the three groups (Fig. 3e). However, the RFP+ propriospinal axons of rats in MN-MSC group were higher than that of rats in the other groups, indicated by the images of coronal sections of spinal segments below the injury sites (Fig. 3f).

Then, we stained the serotonergic axons and ubiquitous axonal fibers with anti-5-hydroxy tryptamine (5-HT) and anti-neurofilament (NF) in the spinal sections respectively. We found that the trends of 5-HT and NF staining results were similar to RFP

staining (Fig. 3d, S5a). No significant difference between NF and 5-HT could be found above the injury site in the three groups (Fig. 3e, S5b). On the contrary, the rats in the MN-MSC group had more serotonergic axons (stained by 5-HT) and axonal fibers (stained by NF) below the injury site than that of rats in the other two groups (Fig. 3h, S5c), indicating that more propriospinal axons survive after SCI with the MN-MSC patch treatment. In contrast to the control and MN-EXO patch treated rats, we only found axons that extended into the spinal lesion site in the examined subjects with the MN-MSC treatment (Fig. 3c, 3c1, 3c2, 3d, 3d1, 3d2, S5a, S5a1, S5a2), suggesting that the microenvironment with MN-MSC patch treatment was more permissive for axon regrowth. In addition, we did not observe apparent effects of the MN-MSC patch treatment on the other organs (Supplementary Fig. S6), suggesting that this treatment is safe for treating SCI.

3.5 The Remanent of Spared Axons Mediates Hindlimb Locomotor Functional Recovery

After verifying that more spared axons could be rescued by MN-MSC patch treatment, we sought to figure out whether these axons could mediate hindlimb locomotor functions. To this end, we analyzed the hindlimb performance of the rats (three groups) with the Basso, Beattie, and Bresnahan (BBB) scale in a double-blind manner. We found that the rats in the control and MN-EXO groups exhibited paralysis with occasional ankle movement during the observation period, with an average BBB score of less than 4 (Fig. 4c). Even though the rats in the MN-MSC group were predominantly demonstrated paralyzed hindlimbs during the first 4 weeks and showed no significant difference from the control and MN-EXO groups (Fig. 4c), they showed vigorous knee and ankle movement at 5 weeks. The BBB score was significantly higher than that of rats in the other two groups after 5 weeks post-injury. More strikingly, at the 8th week after SCI, the rats treated with MN-MSC patch improved their hindlimb motor, with higher body weight support and stride length than that of the rats in the other two groups (Fig. 4c, d, f, g). Remarkably, we found 4 of 10 rats in the MN-MSC patch treated group showed the ability of sustained weight support with hindpaw plantar stepping, and the BBB score had reached more than 10, which has never been observed in the rats in the control or the MN-EXO groups (Fig. 4b, Supplementary Movie S1). Moreover, through subsequent analysis of the 7 kinds of hindlimb kinematics of rats in the groups of control, MN-EXO, MN-MSC and Intact, we found that the MN-MSC patch treatment could increase the maximal height of the iliac crest and toe (Supplementary Fig. S7a, b), height amplitude of iliac crest and toe (Supplementary Fig. 7c, d), angle oscillation of hip, knee and ankle (Supplementary Fig. S7e-g). The hindlimb locomotor performance of rats in MN-EXO group was slightly better than those in the control group, but without significant difference (Supplementary Fig. S7a-d). However, the hindlimb locomotor performance of the rats treated

with the MN-MSC patch was significantly better than that of rats in the MN-EXO and control groups but not as good as that of the rats in the intact group, suggesting that the hindlimb functional recovery with this treatment relied on the remanent of spinal connections across the lesion.

To take both features of data distribution and statistical meaning into account in each kinematics indicator, we draw the radar plot (Fig. 4h). While all indicators in each group are divided by the counterpart in the intact group, it is obvious that the amplitudes of crest and toe of the rats in the MN-MSC group are fairly high compared with that of rats in the MN-EXO and control groups (Fig. 4h). But, the maximum heights of the toe and crest of the rats treated with MN-MSC are remarkably higher than that of rats in the MN-EXO and control groups (Fig. 4h), possibly because the crest and toe determine the gait and stride length while walking. Comprehensively considering the value and distribution in each group, we found that the angle amplitudes among ankle, knee and toe of rats in the MN-MSC group remain low, which is consistent with the results of the hindlimb kinematic study (Supplementary Fig. S7a-g).

To further determine the function of the MN-MSC patch treatment, we performed the somatosensory evoked potential (SSEP) monitoring study of the rats during anesthesia (Fig. 5a). Compared with BBB score, SSEP is more direct for measuring the functionality of neuropathway from cortical projections.[23] As expected, we found the SSEP showed a similar trend to the BBB score at the 8th week post-injury (Fig. 5b, c), which confirms the axon protection function of MN-MSC patch treatment. Then we recorded the electromyography (EMG) to assess the rats' hindlimb muscles motion when they were walking. We found that the ankle flexor signals of tibialis anterior (TA) muscles and extensor gastrocnemius soleus (GS) muscles were rarely active in the control group, and the muscle signals of MN-EXO-treated rats could only be occasionally observed. In contrast, alternating activation of the TA and GS for the MN-MSC patch-treated rats could be consistently observed during different steps (Fig. 5d-f). To further analyze the EMG data, the method of astronomical analysis (Poincaré statistical analysis) was used to analyze the rhythm of the TA and GS muscles. We found that the rhythms of TA and GS muscles of the rats in the MN-MSC group were higher than that of rats in the control and MN-EXO groups with a wider distribution range of scatter points and more concentrated at the central points (zero) position, which were more similar to the ones of the intact group (Supplementary Fig. S8), suggesting that those rats gain much better muscle control through MN-MSC patch treatment. From this, we explored why the gait of rats treated with MN-MSC patch were closer to normal ones. Altogether, these results suggested that rescued axons by the MN-MSC patch treatment could mediate robust hindlimb locomotor functional recovery.

4. Discussion

In this study, we constructed a novel MN-MSC patch that can deliver MSC-EXO sustainedly from the MSC-embedded patch to the spinal tissues in the injury site and avoid the risk of direct stem cells invading into the spinal cord. The MN component of the patch was made of porous GelMA hydrogel with a good biocompatibility and the patch can keep on top of the spinal lesion for long-term to cover the optimal therapeutic window, achieving the maximum therapeutic efficacy of an MSC-EXO treatment.

The study proposed a novel MN-MSC patch for SCI treatment, which could avoid additional surgical damage to the injured spinal cord and provide sustained high-effective MSC-EXO release. As we know, the retention time of MSC-EXO in an alive subject is short, but treatment with MSC-EXO for at least 7 days after SCI is required to prevent secondary injury.[21, 24] Moreover, the direct injection of MSC-EXO or biomaterials containing MSC-EXO into the lesion of an acute SCI is not ethically acceptable due to unpredictable clinical accidents. In comparison with these traditional treatment methods with MSC or MSC-EXO for SCI, the MN-MSC patch seeded with MSC could avoid this ethical issue and provide an ethically acceptable method to deliver MSC-EXO sustainedly for at least 7 days after SCI, which efficiently modulates dysregulated neuroinflammation after SCI and protects spared tissue/axons from secondary injury.[21] In comparison with the traditional local injection methods, the method provided by this study topically delivers the MSC-EXO with low immunogenicity and high safety[25] to the spinal injury site through the porous MN structure with higher accuracy and efficiency.

Our findings showed that the MN-MSC patch treatment could promote functional recovery by protecting the spared axons from secondary injury. In this study, the results of anatomical and functional recovery were analyzed in a double-blinded manner, ensuring the authenticity and effectiveness of the data. Consistent with the MSC-EXO function of immune modulation, apoptosis inhibition and enhanced angiogenesis[9c, 9d, 26], more vessels（CD31, Arg-2）formed in the spinal lesion of SCI rats with our treatment, which can supply sufficient nutrients and oxygen to remodel the SCI microenvironment and then protect the spared axons.[27] Furthermore, the spinal cord of rats treated with MN-MSC patch showed less inflammation (Iba1, MMP-9) with more neurons (NeuN), less apoptosis and death of spinal cord cells (Bax), and more myelin sheath (MBP), which benefit plasticity of spinal circuitry toward functional. By axon tracing and labelling, we showed that more axons survived from secondary injury by MN-MSC patch treatment. In comparison with the rats in the control or MN-EXO treatment groups, the rats with MN-MSC patch treatment exhibit remarkable hindlimb locomotion functional recovery, which is consistent with their better muscle control ability, indicated by the PPV and signal of TA and GS muscles EMG recording studies.

Even though we proved the efficacy of the MN-MSC patch for SCI treatment, the optimal time window for MN-MSC patch implantation remains to be examined. Since the MN-MSC patch was fabricated from GelMA hydrogel, we envisioned that the MN-MSC patch would degrade in the long term;[28] however, when the materials of the MN-MSC patch could totally degrade remained to be investigated by future studies. In addition, the relationship between the number of exosomes released from the MN-MSC patch and the best treatment effect has not been tested, which needs to be investigated before clinical study. To promote the diffusion and improve delivery efficiency, in our next step, we plan to construct a precise porous microneedle structure at micro/nano scale with two-photon 3D printing technology, which might have higher precision in controlling the porous size of the microneedles.[29] Moreover, the MN-MSC patch might be too soft to be used as an artificial dura for clinical SCI treatment, and a tenacious MN-MSC patch with adding a scaffold structure between the MN array and the MSC-embedded patch is under development by our group.

Methods

Animals

Female Sprague-Dawley rats (220-250 g) were purchased from the Zhejiang Academy of Medical Sciences. All experiments were approved by the Zhejiang University School of Medicine Animal Experimentation Committee (approval ID: ZJU20210110). The rats were housed under controlled environmental conditions and were completely in compliance with the National Institutes of Health Guide for the Care and Use of Laboratory Animals. All surgeries were done under anesthesia with 1% (w/v) pentobarbital sodium (5 mL/kg, injected intraperitoneally).

Materials

Chicken anti-GFAP [abcam (ab1344360, 1:500)], rabbit anti-neurofilament (NF) heavy polypeptide [abcam (ab8135), 1:500], goat anti 5-HT antibody [Invitrogen (pa1-36157), 1:500], rabbit anti-NeuN [abcam (ab177487), 1:1000], rabbit anti-MBP [abcam (ab218011), 1:500], goat anti-IBA1 [abcam(ab5076), 1:500], rabbit anti-CD31 [rd system (AF3628), 1:500], human Specific GAPDH Rabbit mAb [ABclonal (AB 2769571,1:500)]. Adenovirus-associated virus, AAV2/9-hSyn-mCherry, was generated by the viral core of Zhejiang University, and its titer was adjusted to 1×10^{13} copies per mL for injection. Donkey anti-chicken secondary antibody conjugated with Alexa Fluor 488, donkey anti-rabbit IgG (H+L) highly cross-adsorbed secondary antibody conjugated with Alexa Fluor 555, and rabbit anti-goat secondary antibody conjugated with Cy3 were purchased from Abcam (USA). Rabbit/mouse-specific antibodies conjugated with HRP [Beyotime (A0208), 1:1000]. DAPI-containing antifade mounting medium was purchased from SouthernBiotech (0100-20, USA)

Preparation of MSC

Human ESC (embryonic stem cell) derived MSCs were generated by Ysbiotech, Hangzhou , China (YS™ hESC-MSC), and cultured at 37 °C in a humidified atmosphere of 5% CO_2 in serum-free medium for mesenchymal stem cells (NC0103+NC0103.S, Yocon, Beijing, China) as previously reported[30] with some modification. When the proliferating colonies had reached near-confluence, the hESC-MSCs were passaged using stem cells moderate digestive enzymes (NC1004, Yocon, Beijing, China). After 3-4 passages, MSCs were used for transplantation or other investigations.

Fabrication and Characterization of the Microneedle array

The MN arrays were fabricated with polydimethylsiloxane molds (EFL-MMN-600) from EFL Ltd. The MN has a 250-μm-diameter, which tapers for a height of 600 mm. The MN arrays were arranged 550 um, tip to tip, in a 4 mm×4 mm area. First, 5% porous GelMA (EFL-GM-pr-001) solution was prepared in a 37℃ water bath and dropped into the molds. Next the bubbles of the casting solution were removed by vacuum pumping, and the molds were placed in a 37℃ environment for 10 h to dry. Then the casting solution was solidified with blue light curing (405 nm, 30mW/cm^2) in 30s. After that, the MN was separated from the molds with tweezers cautiously. The MN array was cut into small pieces at the scale of 3mm×3mm. The morphology of the MNs was assessed with a scanning electron microscope (SEM) (Thero FEI, Nova Nano 450).

Fabrication and Characterization of the MN-MSC Patch

First, the MSCs were digested by Stem cells digestive enzymes (NC1004.1) and mixed in 5% porous GelMA solution evenly in the ratio of 2.5×107cells/mL at 37℃. Next, the solution was added to the basal side of MN array and the MN-MSC patch was got with a blue light curing process for 30s. The MN-MSC patch was cultured in MSC Serum Free Media.

The viability of MSCs in the MN-MSC patch was evaluated with a Live/Dead viability/cytotoxicity kit. After washing the MN-MSC patch with PBS, the MSCs were stained with 0.2% Ethidium homodimer-1 and 0.05% Calcein AM in PBS for 20min. Then the MN-MSC patch was washed three times and observed by laser scanning confocal microscope (Nikon, A1R). The proliferation of the MSCs in the MN-MSC patch was tested by CCK8 assay on 1st, 3rd and 5th day. MN-EXO is fabricated with the similar way with MSC secreted exosomes (1.25 μg/μl) instead of MSC.

Surgical Procedure

For the *in vivo* experiments, a spinal contusion injury model was induced by an Infinite Vertical impactor (68099, RWD, China). Specifically, after being anesthetized, a laminectomy at the tenth thoracic vertebral level (T10-11) of a rat was performed to expose the dorsal surface to induce spinal cord injury.[31] Next, contusion was performed using a cylinder (diameter, 3 mm) that impacted the spinal cord at a rate of 2.5 m/s and was left 5 s at a depth of 2 mm after being impacted (Supplementary Fig. S2a, b). After 3 hours, the dura mater at the lesion site was cut carefully using micro scissors (S11001-09, RWD, China) in the direction of the spinal cord and microneedle was placed at the site of the dura matter defect (Supplementary Fig. S2c, d). GelMA with MSCs (25,000 cells/μL) was dripped onto the microneedle and irradiated with light at a wavelength of 405 nm for 1 minute to get the MN-MSC patch (Supplementary Fig. S2e). Then, 5% GelMA solution was continued to drip on the surface of the exposed spinal cord with the patch and gelled with blue light to fix the

patch on the injury site of the spinal cord (Supplementary Fig. S2f-h). The control group rats underwent contusion and dura mater cutting, but no microneedle was placed. The surgery of MN-EXO implantation was performed on the same way with MSC secreted exosomes (1.25μg/μl) instead of MSC. Artificial micturition was provided twice daily until the automatic restoration of bladder voiding.

At 6 weeks after injury, anterograde tracing of propriospinal axons was performed via the injection of AAV2/9-hSyn-mCherry at the T7-8 spinal cord[32]. Specifically, a pull-glass micropipette tipped 10-μL Hamilton microsyringe (68606, RWD, China) was used for precisely injecting. After a laminectomy was performed at the T7-8 spinal cord, AAV2/9-hSyn-mCherry was injected into 12 sites following the coordinates: 1) 0.4 and 0.8 mm lateral to the midline; 2) 0.5, 1.0 and 1.6 mm from the surface. The injecting rate is 80 nl/min and the injected liquid is 150 nl per sites. The needle was left for 1minute before moving to the next. Animals were sacrificed for assessment 2 weeks after injection.

Evaluation of MSC- EXO Release Profile of the MN-MSC Patch

To evaluate the advantage of the release function of the MN-MSC patch, we measured the MN-EXO patch release capacity (contained EXO instead of MSC) against the capacity of our MN-MSC patch. The patches were cultured and placed on the surface of culture inserts (Fig. 1i) to investigate the MSC-EXO release function of the two different patches. The released MSC-EXO in the culture medium was quantified with Micro BCA Protein Assay kit.[17] The MSC-EXO was collected from the supernatant using ultracentrifugation. The size and morphology of MSC-EXO were tested with Transmission electron microscopy (TEM, Nova Nano 450).

Because the MSC-EXO released from the MN-MSC patch is hard to be examined visually, we used the CM-DiI-MN-EXO patch (EXO labeled with CM-DiI) to observe the *in vivo* release capability of the MN patch. The CM-DiI-MN-EXO patch was implanted in the injuried spinal cord of the rat. The method of patch implanting had been described in the part of animal and surgical procedures. The stained Images of the EXO released in the SCI were acquired by a slide scanner (VS200, Olympus, Japan).

Histochemistry

Animals were sacrificed at 8 weeks after injection for histological assessment. After the animals were anesthetized, perfusion was performed using PBS and 4 %paraformaldehyde. Spinal cords and other tissues were fixed in 4% paraformaldehyde overnight and dehydrated with sucrose for 1 day. After being embedded using optimal cutting temperature compound

(OCT), twenty-micrometer-thick sections of the spinal cord were cut using a cryostat (CryoStar NX50; Thermo, USA) and mounted onto slides.

For immunofluorescence histochemistry, spinal cord tissue sections were blocked with 5% donkey serum for 1 hour and incubated with primary antibodies overnight at 4℃. After washing with PBS three times, the tissues were incubated with secondary antibodies conjugated to fluorescent dyes for 2 hours at room temperature. Then, tissues were rewashed with PBS and dripped with an antifade mounting medium containing DAPI. Images was acquired by a confocal laser scanning microscope (A1Ti, Nikon, Japan) and a slide scanner (VS200, Olympus, Japan).

For immunohistochemistry, tissue sections were stained with hematoxylin and eosin (H&E). Images were acquired by a slide scanner (VS200, Olympus, Japan).

Western blotting

Cells were washed three times with ice-cold PBS and lysed in RIPA buffer containing 1% PMSF. After leaving on ice for 30 min, samples were centrifuged at 12000 g for 15 min at 4 ℃. Protein concentrations in the supernatant were assessed using the bicinchoninic acid protein assay kit (Beyotime, China). Equal amounts of protein extracts were resolved by 10%-12% SDS-SPAGE and electro-transferred onto the polyvinylidene (Bio-Rad, USA). After a blockade in Tris-buffered saline plus 5% (w/v) milk, membranes were exposed to primary antibodies overnight at 4 ℃. Secondary antibodies conjugated to horseradish peroxidase were incubated with samples for 1 hour at room temperature. Signals were visualized by Chemi DocXRS + Imaging System (Bio-Rad, USA), and ImageJ software was used to assess gray levels. All experiments were repeated three times.

Behavioral assessment

The locomotion performances of rats were recorded by a camera once a week during the experiments. An examiner blinded to the treatment assessed the videos recording the rats' behavioral performance by the Basso, Beattie Bresnahan rating scale (BBB scale).[33] Rats that showed a BBB score above 1.5 at 1 week after SCI were excluded from further histological or behavioral analysis. To precisely understand the locomotor kinematics, the representative hindlimb osteoarticular landmarks (toe, ankle, knee, hip, and crest) were labeled by 5 mm reflective balls and tracked by the Infrared 3D Motion System (Vicon Nexus,

UK).[20] Typical sequential treads and the ankle degrees of selected articulates were displayed. Meanwhile, the body weight support and the stride length were compared as previously introduced[33].

The behavioral data was depicted with seven features (maximal iliac crest height, crest height amplitude, maximal toe height, toe height amplitude, hip, knee and ankle angle oscillation) within four groups (intact, control, MN, MN-MSC). For each group, we utilized different statistical methods to calculate seven behavioral features, these features have different units as well. As we need to well-rounded analysis these features together in radar graph, normalizing these data is vital and pivotal. First and foremost, for each value in each feature, we normalize the seven behavioral feature data by the equation (1):

$$\widetilde{x_i} = \frac{(x_i - \bar{x})}{\sqrt{\sigma}} \#(1)$$

where x_i serves as the ith data in each seven-behavioral-feature, $i = 1,2,3,\ldots n$. n is the numbers of points sampling from each feature in each group; $\bar{x}$ and $\sqrt{\sigma}$ serve as the mean value and standard variance of each feature, respectively.

Secondly, we get the seven $\widetilde{x_i}$ Each group has positive and negative values, and the scale among these values is not fixed. Hence, we project the features into exponentiation expression, mapping these values in a unified scale (a unified vector space). For each feature depicted in a different group, we use the equation (2) to process this step:

$$\widetilde{x_f} = \frac{average(e^{\widetilde{x_i}})}{max(average(e^{\widetilde{x_i}}))} \#(2)$$

where $f = 1,2,3,\ldots,7$, serves as the seven behavioral features in each group. As we average the $e^{\widetilde{x_i}}$ in each group, obtaining lists with seven features values in each group.

And in the final analysis, we use the intact group values as the benchmark, significantly depicting the feature values' variance. We use the equation (3) to process this step:

$$\tilde{x}_o = \frac{\tilde{x}_g}{\tilde{x}_{intact}} \#(3)$$

where $\tilde{x}_g$ serves as each feature value in each group. $\tilde{x}_{intact}$ serves as the feature values in the intact group, namely, the benchmark values.

Implantation of electrodes

Electrode implantation was performed 8 weeks after SCI for both evoked potential and hindlimb EMG according to previous protocols.[20, 34] Rats were anesthetized by

dexmedetomidine hydrochloride (0.25 mg/kg i.p.; MCE, US) and 0.5% isoflurane, which worked well on the acquisition of evoked potential.[34a] A stainless steel screw electrode was fixed on the skull above the hindlimb region stereotactically (B-2.0/R+2.5/D-0.7) for an epidural recording of cortical evoked potential referring to the zero potential on the shoulder (ground lead connected to B-6.0/R4.0).[34b] Following the somatosensory evoked potential (SSEP), bipolar electrodes (AS632, Conner wire) were inserted into the right medium gastrocnemius (GS) and tibialis anterior (TA) for *in vivo* assessment of hindlimb muscles with the reference lead linked to the ipsilateral tendon.[20] Wires were subcutaneously connected to the header plate fixed on the skull.

SSEP recording and processing

During the surgery, the header was connected with a neuron signal amplifier (BTAM01L, Braintech, China) and the signal was recorded by a Neurostudio system (Braintech, China) [20]. A series of pulses (2.0 Hz, 2.0 mA, 0.5 ms) was applied to the left hindlimb paw through a pair of electrodes by a neurostimulator (BTSEM-16, Braintech, China) under anesthesia[34a]. Signals were obtained from a five-minute stimulation, followed by a 30- to 1500- Hz bandpass, the power line noise notch filtration (50 Hz and the two consequent harmonics 100 Hz, 150 Hz), and the removal of stimulation artifacts. Then the first 150 qualified trials were chosen for peak-to-peak potential (PPV) calculation. PPV was normalized according to the intact group, following the method described by Gunnar Waterstraat et al.[35]

EMG recording and processing

Seven days post-implantation, five osteoarticular structures were captured to distinguish stance and swing when moving freely and the header was connected up to the amplifier for detecting the muscle strength. Next, the free-moving muscle activity, represented by an extensor and a flexor of the right hindlimb, was logged in the Neurostudio. Data were filtered (band pass 20Hz-1000 Hz) before computing the muscle amplitude on the MATLAB platform.[34c]

Statistics

Statistical analysis was performed on python 3.9.7. The Sharpiro and Bartlett tests were performed to verify the normal distribution and the homogeneity of variance, separately. One-way ANOVA with inter-group comparison (Bonferroni corrected t test) was used. All parameters were expressed as the mean ± SEM and the significance level was below 0.05.

Acknowledgments

This study was supported by the Scientific and Technological Innovation 2030 Program of China -

major projects (2021ZD0200408 to X.W.), the National Natural Science Foundation of China (81971866 to X.W.), the Science Fund for Distinguished Young Scholars of Zhejiang Province (LR20H090002 to X.W.), the Leading Innovative and Entrepreneur Team Introduction Program of Zhejiang (2019R01007 to X.W.), the Fundamental Research Funds for the Central Universities (K20210195 to X.W.) and the Postdoctoral General Foundation project (2020M671746 to X.C.).

Conflict of Interest

Zhejiang University has filed a patent application related to this work, with X.W., A.F., and B.G. listed as inventors.

Author Contributions

A.F., Y.W., and N.G. contributed equally to this work. X.W., and A.F. conceptualized and designed the study. A.F., Y.W., and N.G. conducted the experiments and collected the data. A.F., Y.W., and N.G., L.L, B. G., W. C., X.C. J. Y., S.J., X. G., X.G., B.Y. and X.W. analyzed and interpreted the data. A.F. and X.W. drafted the paper. All authors critically revised the manuscript and approved the final version for submission.

Data Availability Statement

The data to support the findings of this study are included in the paper and supplementary information, and further data are available from the corresponding author upon reasonable request.

References

[1] G. B. D. M. S. Collaborators, *The Lancet. Neurology* **2019**, 18, 269.

[2] a)D. Short, *Bmj* **2000**, 321, 1224; b)Y. T. Wu, T. Y. Li, H. Y. Chu, L. C. Chen, S. L. Chiang, S. T. Chang, *Neurosciences (Riyadh)* **2011**, 16, 324; c)T. Matsumoto, T. Tamaki, M. Kawakami, M. Yoshida, M. Ando, H. Yamada, *Spine* **2001**, 26, 426.

[3] S. Christopher, Ahuja, R. Jefferson, Wilson, Satoshi, Nori, R. N. Mark, Kotter, Claudia, Druschel, *Nature reviews. Disease primers* **2017**.

[4] M. Bains, E. D. Hall, *Biochimica Et Biophysica Acta* **2012**, 1822, 675.

[5] a)A. M. Akhtar, S. Al, A. H. Eid, *Frontiers in Cellular Neuroscience* **2016**, 10; b)F. Tahmasebinia, A. Pourgholaminejad, *Progress in neuro-psychopharmacology & biological psychiatry* **2017**, 408.

[6] A. Shao, S. Tu, J. Lu, J. Zhang, *Stem Cell Research Therapy* **2019**, 10.

[7] a)L. Huang, C. Fu, F. Xiong, C. He, Q. Wei, *Cell transplantation* **2021**, 30, 963689721989266; b)S. Yao, F. He, Z. Cao, Z. Sun, Y. Chen, H. Zhao, X. Yu, X. Wang, Y. Yang, F. Rosei, L. N. Wang, *ACS Biomater Sci Eng* **2020**, 6, 1165; c)S. W. Wong, S. Lenzini, M. H. Cooper, D. J. Mooney, J. W. Shin, *Sci Adv* **2020**, 6, eaaw0158; d)L. Zhang, C. Fan, W. Hao, Y. Zhuang, X. Liu, Y. Zhao, B. Chen, Z. Xiao, Y. Chen, J. Dai, *Advanced healthcare materials* **2021**, 10, e2001896; e)M. Nakazaki, T. Morita, K. L. Lankford, P. W. Askenase, J. D. Kocsis, *Journal of extracellular vesicles* **2021**, 10, e12137.

[8] H. S. Chhabra, K. Sarda, *Advanced Drug Delivery Reviews* **2017**, 120, 41.

[9] a)G. Ren, L. Zhang, Z. Xin, G. Xu, Y. Zhang, A. I. Roberts, R. C. Zhao, Y. Shi, *Cell Stem Cell* **2008**, 2, 141; b)M. Gnecchi, H. He, O. D. Liang, L. G. Melo, F. Morello, H. Mu, N. Noiseux, L. Zhang, R. E. Pratt, J. S. Ingwall, *Nat Med* **2005**, 11, 367; c)S. Zhang, S. J. Chuah, R. C. Lai, J. H. P. Hui, S. K. Lim, W. S. Toh, *Biomaterials* **2018**, 156, 16; d)S. Bian, L. Zhang, L. Duan, X. Wang, Y. Min, H. Yu, *Journal of molecular medicine* **2014**, 92, 387; e)J. Rehman, D. Traktuev, J. Li, S. Merfeld-Clauss, C. J. Temm-Grove, J. E. Bovenkerk, C. L. Pell, B. H. Johnstone, R. V. Considine, K. L. March, *Circulation* **2004**, 109, 1292.

[10] a)L. Li, Y. Zhang, J. Mu, J. Chen, C. Zhang, H. Cao, J. Gao, *Nano letters* **2020**, 20, 4298; b)J. Mu, L. Li, J. Wu, T. Huang, Y. Zhang, J. Cao, T. Ma, J. Chen, C. Zhang, X. Zhang, *Biomaterials Science* **2022**, 10, 1803.

[11] a)S. S. Ousman, P. Kubes, *Nature neuroscience* **2012**, 15, 1096; b)M. L. Block, L. Zecca, J. S. Hong, *Nature reviews. Neuroscience* **2007**, 8, 57.

[12] a)Z. Lv, C. Dong, T. Zhang, S. Zhang, *Frontiers in bioengineering and biotechnology* **2022**, 10, 931800; b)C. Chen, X. Qiao, W. Liu, C. Fekete, J. D. Reinhardt, *Spinal cord* **2022**; c)J. Li, D. J. Mooney, *Nat Rev Mater* **2016**, 1; d)N. Mukherjee, A. Adak, S. Ghosh, *Soft matter* **2020**; e)L. Afferi, J. Pannek, A. Louis Burnett, C. Razaname, S. Tzanoulinou, W. Bobela, R. A. F. da Silva, M. Sturny, N. Stergiopulos, J. Cornelius, M. Moschini, C. Iselin, A. Salonia, A. Mattei, L. Mordasini, *Andrology* **2020**, 8, 1660; f)S. Santi, I. Corridori, N. M. Pugno, A. Motta, C. Migliaresi, *ACS Biomater Sci Eng* **2021**, 7, 983; g)B. Brommer, M. He, Z. Zhang, Z. Yang, J. C. Page, J. Su, Y. Zhang, J. Zhu, E. Gouy, J. Tang, P. Williams, W. Dai, Q. Wang, R. Solinsky, B. Chen, Z. He, *Nature Communications* **2021**, 12, 781.

[13] D. Macaya, M. Spector, *Biomedical materials* **2012**, 7, 012001.

[14] a)J. Tang, J. Wang, K. Huang, Y. Ye, T. Su, L. Qiao, M. T. Hensley, T. G. Caranasos, J.

Zhang, Z. Gu, *Science Advances* **2018**, 4, eaat9365; b)G. Yang, Q. Chen, D. Wen, Z. Chen, J. Wang, G. Chen, Z. Wang, X. Zhang, Y. Zhang, Q. Hu, *Acs Nano* **2019**, 13, 4354; c)X. Zhou, Z. Luo, A. Baidya, H. j. Kim, C. Wang, X. Jiang, M. Qu, J. Zhu, L. Ren, F. Vajhadin, *Advanced healthcare materials* **2020**, 9, 2000527; d)J. Arya, S. Henry, H. Kalluri, D. V. McAllister, W. P. Pewin, M. R. Prausnitz, *Biomaterials* **2017**, 128, 1.

[15] X. Zhou, Z. Luo, A. Baidya, H.-j. Kim, C. Wang, X. Jiang, M. Qu, J. Zhu, L. Ren, F. Vajhadin, P. Tebon, N. Zhang, Y. Xue, Y. Feng, C. Xue, Y. Chen, K. Lee, J. Lee, S. Zhang, C. Xu, N. Ashammakhi, S. Ahadian, M. R. Dokmeci, Z. Gu, W. Sun, A. Khademhosseini, *Advanced Healthcare Materials* **2020**, 9, 2000527.

[16] M. F. Dvorak, V. K. Noonan, N. Fallah, C. G. Fisher, C. S. Rivers, H. Ahn, E. C. Tsai, A. G. Linassi, S. D. Christie, N. Attabib, R. J. Hurlbert, D. R. Fourney, M. G. Johnson, M. G. Fehlings, B. Drew, C. S. Bailey, J. Paquet, S. Parent, A. Townson, C. Ho, B. C. Craven, D. Gagnon, D. Tsui, R. Fox, J. M. Mac-Thiong, B. K. Kwon, *J Neurotrauma* **2014**, 31, 1540.

[17] L. Li, Y. Zhang, J. Mu, J. Chen, C. Zhang, H. Cao, J. Gao, *Nano letters* **2020**, 20, 4298.

[18] H. Branscome, S. Paul, D. Yin, N. El-Hage, E. T. Agbottah, M. A. Zadeh, L. A. Liotta, F. Kashanchi, *Front Cell Dev Biol* **2020**, 8, 455.

[19] M. Á. Brennan, P. Layrolle, D. J. Mooney, *Advanced functional materials* **2020**, 30, 1909125.

[20] J. Ye, S. Jin, W. Cai, X. Chen, H. Zheng, T. Zhang, W. Lu, X. Li, C. Liang, Q. Chen, Y. Wang, X. Gu, B. Yu, Z. Chen, X. Wang, *Adv Healthc Mater* **2021**, 10, e2100242.

[21] J. Ye, S. Jin, W. Cai, X. Chen, H. Zheng, T. Zhang, W. Lu, X. li, L. Chen, Q. Chen, Y. Wang, X. Gu, B. yu, Z. Chen, X. Wang, *Advanced Healthcare Materials* **2021**, 10.

[22] S. Ma, N. Xie, W. Li, B. Yuan, Y. Shi, Y. Wang, *Cell Death & Differentiation* **2014**, 21, 216.

[23] A. H. All, H. Al Nashash, H. Mir, S. Luo, *Brain Research Bulletin* **2020**, 156, 150.

[24] H. Prüss, M. A. Kopp, B. Brommer, N. Gatzemeier, I. Laginha, U. Dirnagl, J. M. Schwab, *Brain pathology* **2011**, 21, 652.

[25] Y. Qin, R. Sun, C. Wu, L. Wang, C. Zhang, *International Journal of Molecular Sciences* **2016**, 17, 712.

[26] S. Bruno, C. Grange, F. Collino, M. C. Deregibus, V. Cantaluppi, L. Biancone, C. Tetta, G. Camussi, *PloS one* **2012**, 7, e33115.

[27] a)C. S. Ahuja, J. R. Wilson, S. Nori, M. Kotter, C. Druschel, A. Curt, M. G. Fehlings, *Nature reviews Disease primers* **2017**, 3, 1; b)Y. Cao, Y. Xu, C. Chen, H. Xie, H. Lu, J. Hu, *Stem Cell Research & Therapy* **2021**, 12, 1.

[28] a)S. Heltmann-Meyer, D. Steiner, C. Muller, D. Schneidereit, O. Friedrich, S. Salehi, F. B. Engel, A. Arkudas, R. E. Horch, *Biomedical materials* **2021**, 16; b)K. Yue, G. Trujillo-de Santiago, M. M. Alvarez, A. Tamayol, N. Annabi, A. Khademhosseini, *Biomaterials* **2015**, 73, 254.

[29] J.-F. Xing, M.-L. Zheng, X.-M. Duan, *Chemical Society Reviews* **2015**, 44, 5031.

[30] H. Nakajima, K. Uchida, A. R. Guerrero, S. Watanabe, D. Sugita, N. Takeura, A. Yoshida, G. Long, K. T. Wright, W. E. Johnson, H. Baba, *J Neurotrauma* **2012**, 29, 1614.

[31] B. Chen, Y. Li, B. Yu, Z. Zhang, B. Brommer, P. R. Williams, Y. Liu, S. V. Hegarty, S. Zhou, J. Zhu, H. Guo, Y. Lu, Y. Zhang, X. Gu, Z. He, *Cell* **2018**, 174, 521.

[32] J. Ye, S. Jin, W. Cai, X. Chen, H. Zheng, T. Zhang, W. Lu, X. Li, C. Liang, Q. Chen, Y. Wang, X. Gu, B. Yu, Z. Chen, X. Wang, *Adv Healthc Mater* **2021**, e2100242.

[33] D. M. Basso, M. S. Beattie, J. C. Bresnahan, *Exp Neurol* **1996**, 139, 244.
[34] a)S. Liu, C. Moncion, J. Zhang, L. Balachandar, D. Kwaku, J. J. Riera, J. L. Volakis, J. Chae, *ACS Sens* **2019**, 4, 3175; b)S. Iyer, A. Maybhate, A. Presacco, A. H. All, *J Neurosci Methods* **2010**, 193, 210; c)B. Chen, Y. Li, B. Yu, Z. Zhang, B. Brommer, P. R. Williams, Y. Liu, S. V. Hegarty, S. Zhou, J. Zhu, H. Guo, Y. Lu, Y. Zhang, X. Gu, Z. He, *Cell* **2018**, 174, 521.
[35] G. Waterstraat, R. Körber, J. H. Storm, G. Curio, *Proc Natl Acad Sci U S A* **2021**, 118.

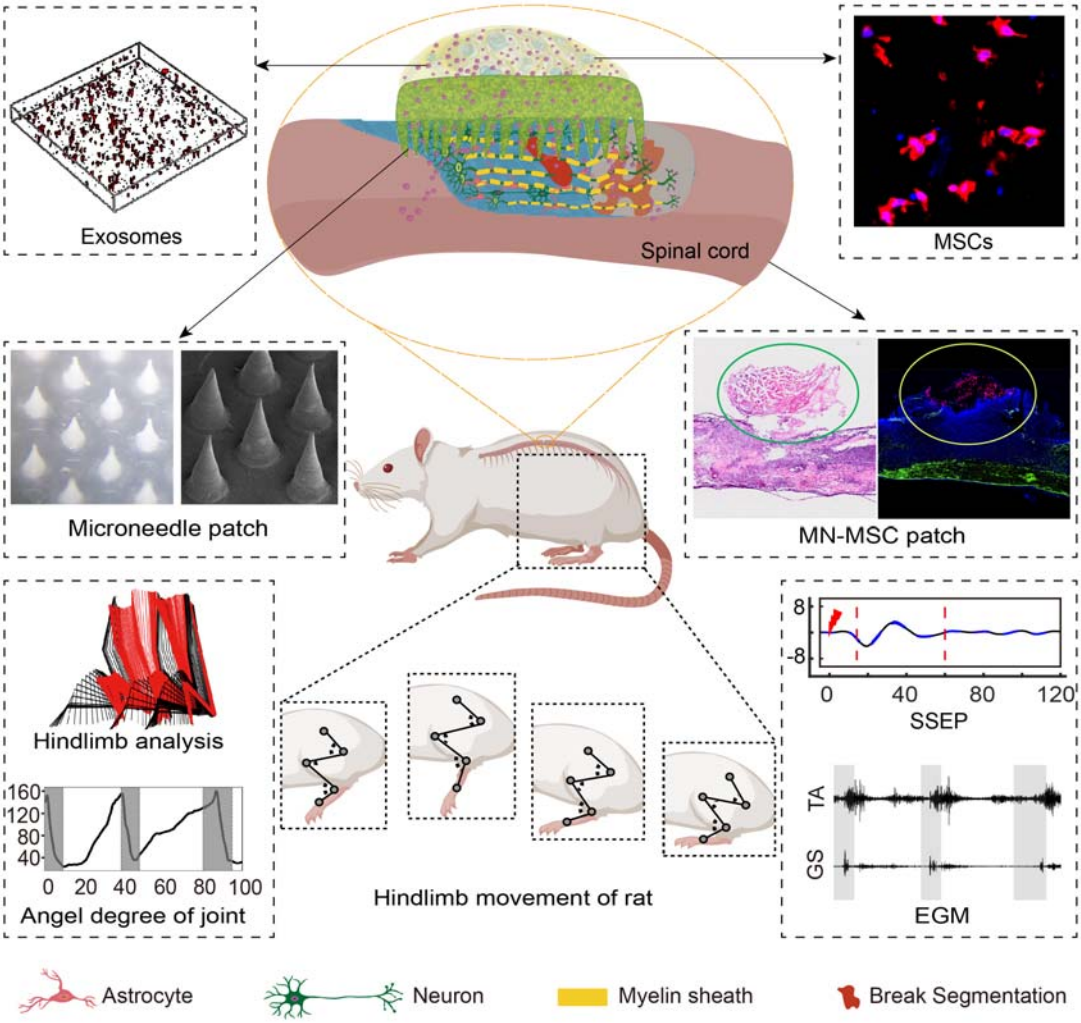

Scheme 1. Schematic illustration of MN-MSC patch implantation on the injury site of spinal cord.

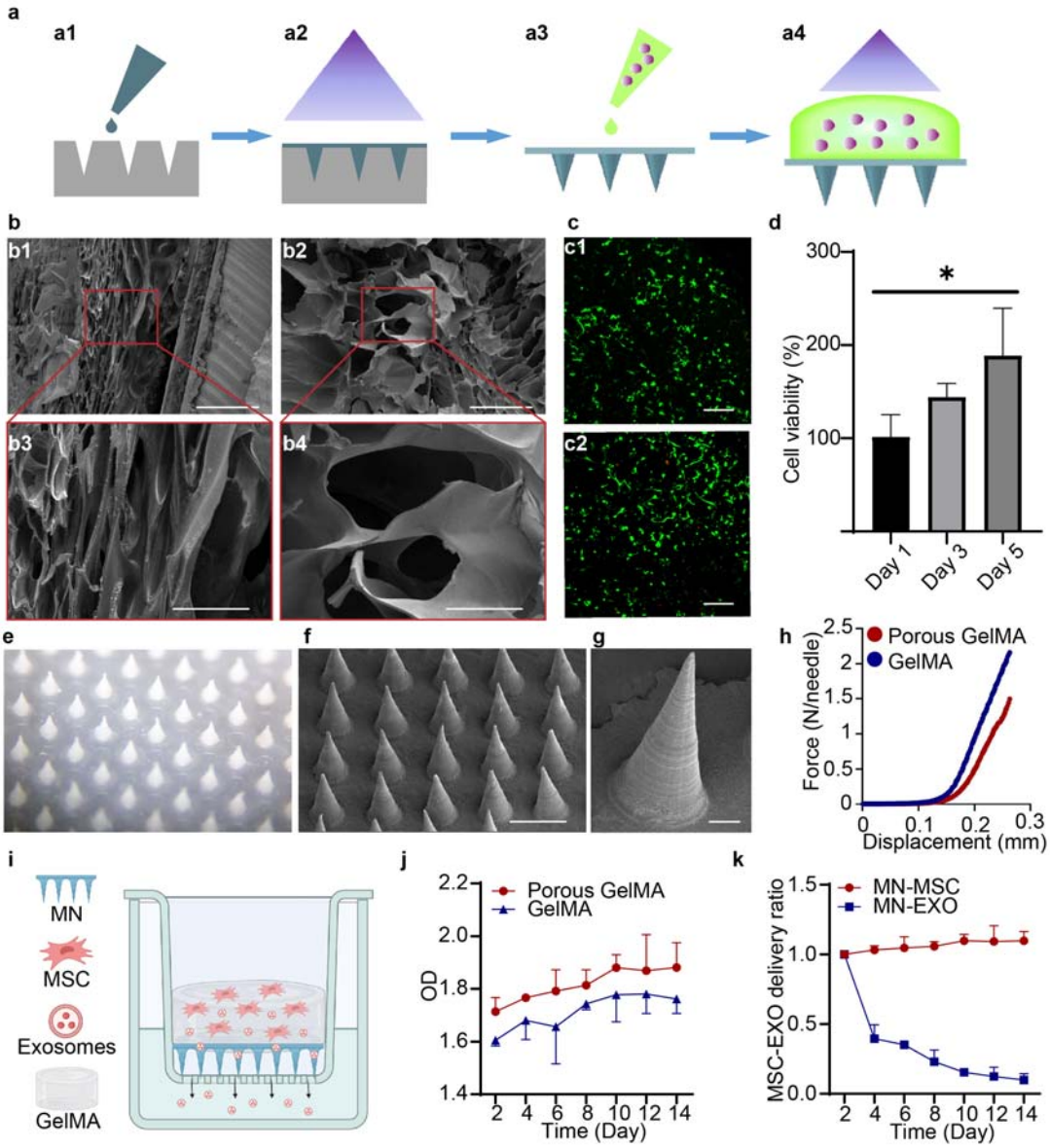

Figure 1. Fabrication and characterization of the MN-MSC patch. a) Schematic of MN-MSC patch fabrication process by a1) casting, a2) blue light crosslinking, a3) peeled off from PDMS mold and adding GelMA solution with MSCs, a4) blue light crosslinking. b) SEM image of b1) interstructure of normal and b2) porous GelMA hydrogel. Scale bars of images (b1, b2) indicate 300µm, and scale bars of images (b3, b4) indicate 100um. c) Calcein (live)/EthD (dead) staining revealed the morphology and viability of MSC encapsulated in GelMA hydrogel on c1) day 3 and c2) day 5. Scale bars: 200 µm. d) The quantitative viability analysis of MSC encapsulated in GelMA hydrogel on days 1, 3 and 5. Data were analyzed with one-way ANOVA followed by Tukey's post hoc test. n=4. *p<0.05. e) Representative optical microscopy images and f-g) SEM (scanning electron microscope) images of MN. Scale bars for images f) indicate 500 µm, and scale bars for images g) indicate 50 µm. h) The

mechanical strength of MN. i) Schematic showing the study design used to test the releasing profile of exosomes from the MN-MSC patch. j) The daily exosome release curves of MN-MSC patch fabricated with porous and normal GelMA hydrogel. Data are presented as means ± SD (n = 3 for each group). k) The daily exosome release curves of MN-MSC and MN-EXO patch. Data are presented as means ± SD (n = 3 for each group).

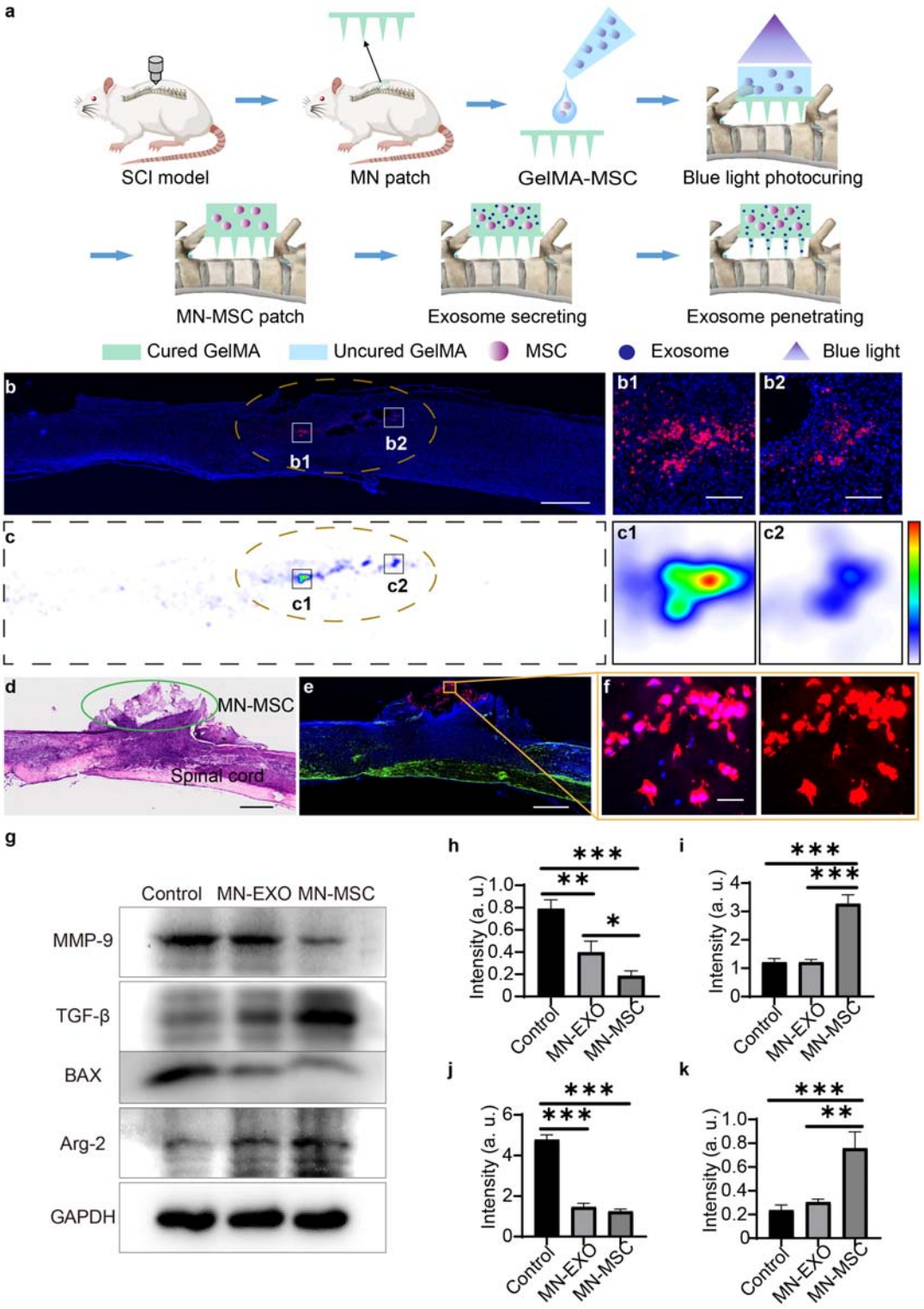

Figure 2. The sustainedly MSC-EXO delivery by MN-MSC patch treatment alleviates neuroinflammation triggered by SCI. a) Schematic illustration of MN-MSC patch implantation on the injury site of the spinal cord. b) In vivo distribution of exosomes (DiI labeled, red) in the

injured spinal cord tissues after MN-EXO patch implantation, blue (DAPI). Scale bar: 1mm. The injury region of the spinal cord was marked with yellow dotted lines. c) The heatmaps of exosome distribution in the injured spinal cord tissues after MN-EXO patch implantation; red: the highest numbers of exosomes, blue: the lowest, white: background. The injury region of the spinal cord was marked with yellow dotted lines. b1, b2, c1, c2) The enlarged images for the details. Scale bar: 100μm. d) HE staining of the injured spinal cord with MN-MSC patch implantation, scale bar: 100μm. e) Representative images of immunohistochemical staining for MN-MSC patch on the injured spinal cord on day 7 after SCI, green (GFAP), blue (DAPI), red (GAPDH), scale bar: 1mm. f) High-magnification images of the box area, scale bar: 50μm. g-k) WB results of quantitative analyses of h) MMP-9, i) TGF-β, j) BAX and k) Arg-2 expression in the injury site of rats in the control, MN-EXO, MN-MSC groups in the first week. Statistical analysis was performed using one-way ANOVA followed Tukey's multiple comparisons test. n=3. **$p<0.01$, ***$p<0.001$.

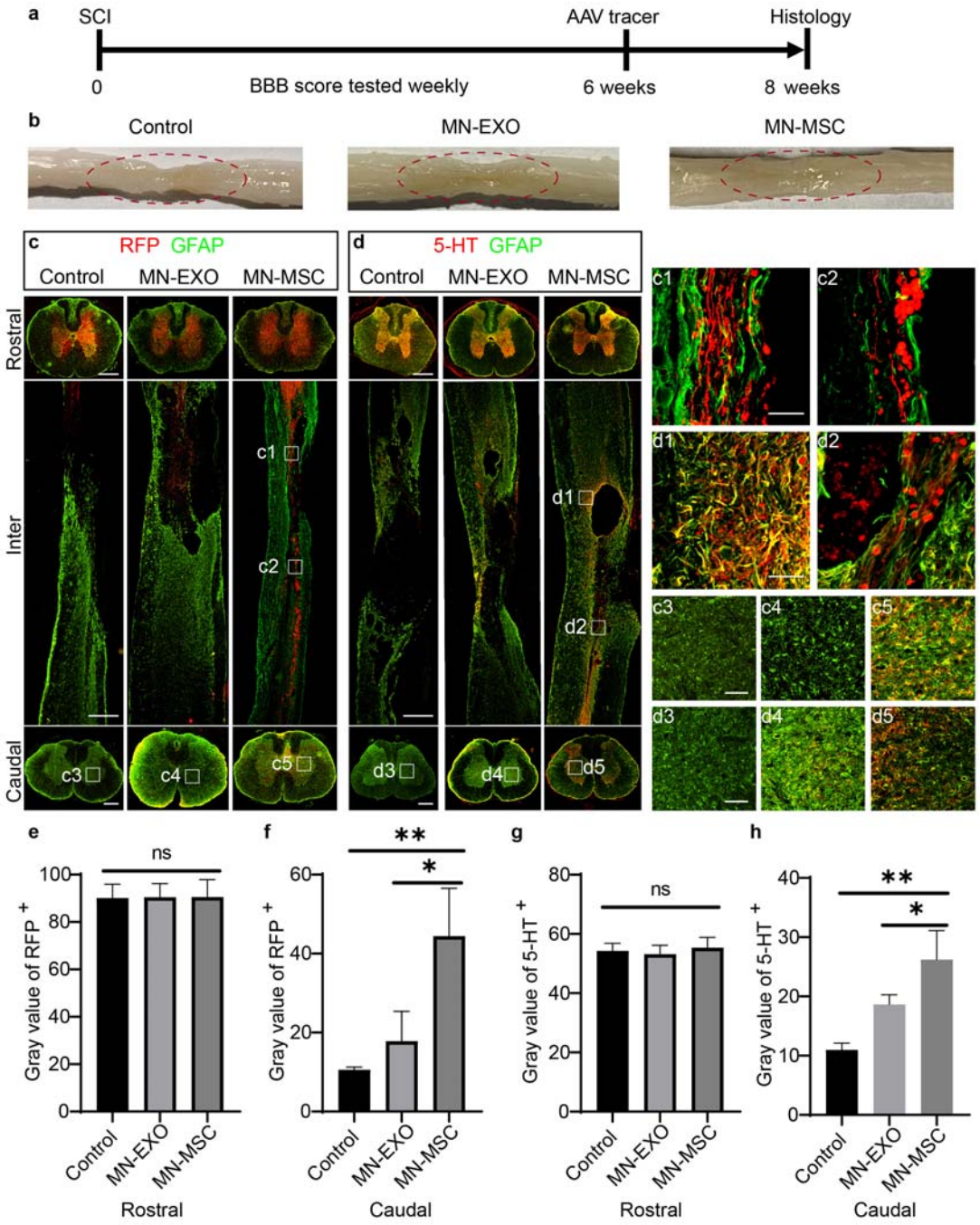

Figure 3. The protection of spared axons with MN-MSC patch treatment after SCI. a) Schematic diagram of the experimental design. MN or MN-MSC patch was implanted 3 hours after SCI, the AAV tracer for axons was injected at 6 weeks, and the histological study was performed at 8 weeks. The locomotion performances of rats were recorded once a week during the experiments. b) Optical images of injured spinal cords of the three groups (control, MN-EXO, MN-MSC) at 8 weeks. Black arrows indicate the injury site. The regions of the injury site are marked with red dotted lines. c, d) Representative images of the spinal sections

stained with GFAP (green), RFP (red), 5-HT (red) of rats in the three groups (control, MN-EXO, MN-MSC) at 8 weeks after SCI. Scale bars of rostral and caudal indicate 500μm, Inter indicate 1mm, c1, c2, d1, d2) indicate 100μm, c3-c5, d3-d5) indicate 100μm. e-h) Quantification of the 5-HT and RFP immunoreactivity gray values on the rostral and caudal sides of the three groups. Data are shown as mean ± SEM. Statistical analysis was performed using one-way ANOVA followed Tukey's multiple comparisons test. Statistical analysis was performed using one-way ANOVA followed Tukey's multiple comparisons test. n = 3. *$p < 0.05$, **$p < 0.01$.

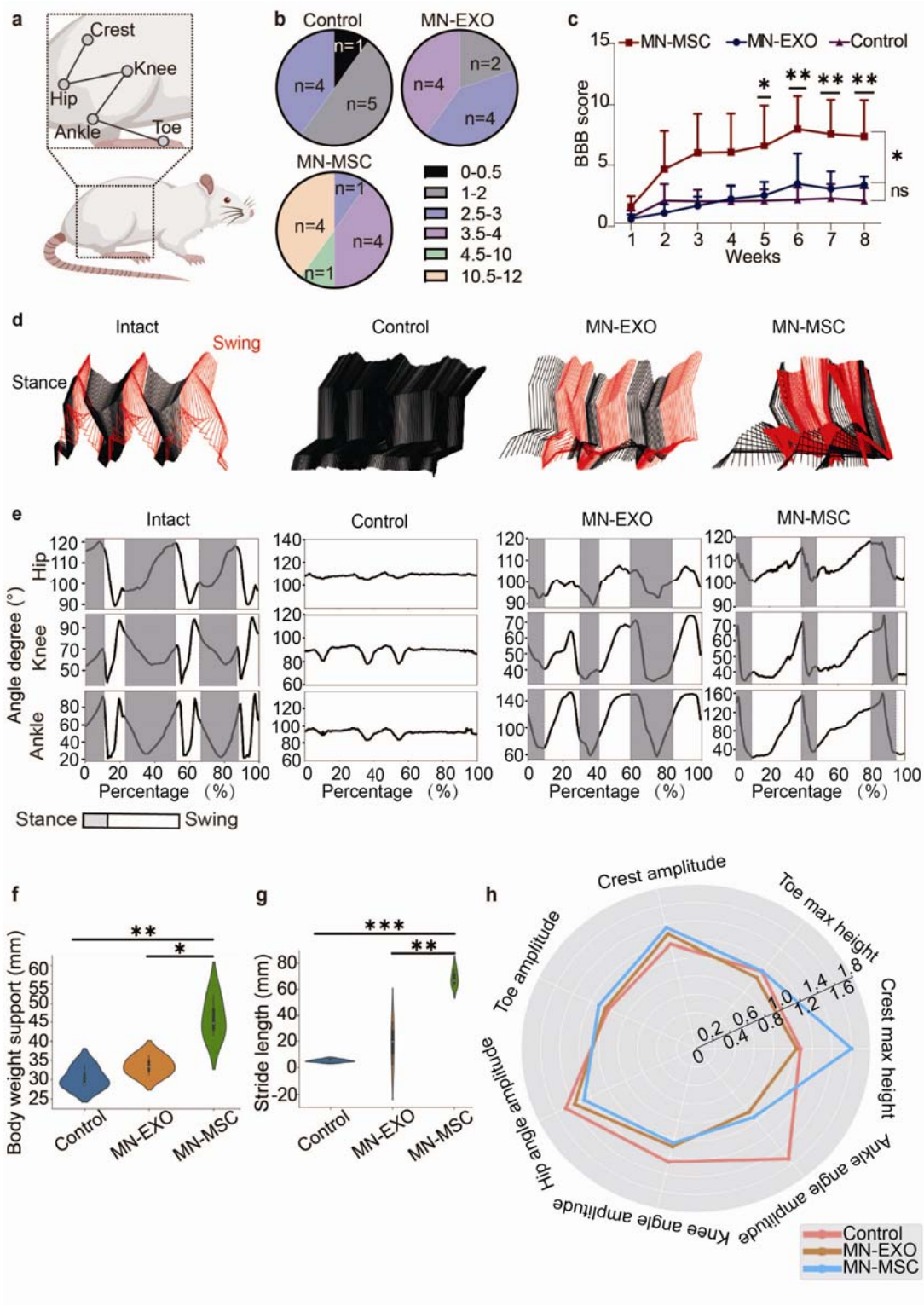

Figure 4. The hindlimb locomotor functional recovery of rats with MN-MSC patch treatments after SCI. a) Schematic illustration of the position of hindlimb crest, knee, hip, ankle and toe. b) The distribution of BBB scores of rats in the three groups (control, MN-EXO, MN-MSC) at 8

weeks after SCI. c) The weekly BBB scores comparison among the rats in the three groups (control, MN-EXO, MN-MSC) at 8 weeks after SCI. One-way ANOVA with Tukey's post hoc test was used for comparisons among multiple groups, and two-tailed paired t-tests were used for comparisons between two groups. n=10. *$p<0.05$ and **$p<0.01$. d) The color-coded stickviews of kinematic hindlimb analysis of the intact rats and the rats with SCI of the groups (control, MN-EXO, MN-MSC). e) The angle degree curves of the ankle, knee and hip of the intact rats and the rats with SCI of the groups (control, MN-EXO, MN-MSC). Quantitative analysis of f) body weight support and g) strike length at 8 weeks. Data were analyzed with one-way ANOVA followed by Tukey's post hoc test. n = 3. *$p < 0.05$, **$p < 0.01$, ***$p < 0.001$. h) Well-rounded quantification of seven described behavioral features in rats of the three groups (control, MN-EXO, MN-MSC), subjected to the indicated treatments through a radar graph.

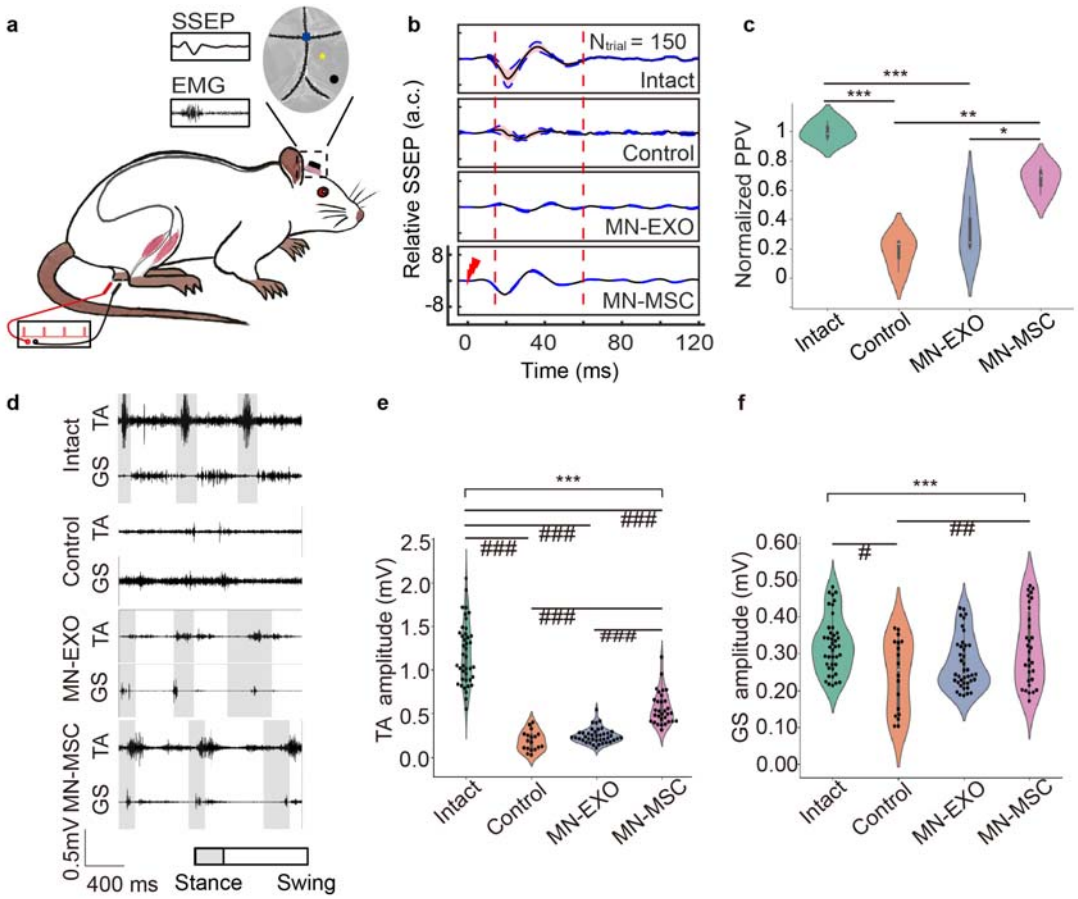

Figure 5. Electrophysiological recording experiments revealed the superior muscle control of rats treated by MN-MSC patches. a) Leads were connected to a pair of antagonistic muscles (TA, tibialis anterior; GS, the medium gastrocnemius) and the epidural electrode above the cortical hindlimb area (marked as a yellow star, B-2/R+2.5/D-0.7) for cortical evoked potential (stimulated by a pair of electrodes on the contralateral hindlimb paw) and free-moving muscle activity, respectively (blue triangular, bregma; black circular, ground lead). b) Representative relative SSEP (somatosensory evoked potential) of each group (N trial = 150) were illustrated as mean (solid black line) and 95% confidence interval (pink shadow enveloped by blue dashed line), the time of electric stimulation was set zero ms. c) Peak-to-Peak potential was analyzed with one-way ANOVA followed by Tukey's post hoc test. n = 3. *p<0.05, **p<0.01, ***p<0.001. d) TA and GS muscle EMG for rats of different groups (intact, control, MN-EXO and MN-MSC). Representative muscle activity of each group was depicted as three consecutive steps, where the gray intervals referred to stance phases. e, f) Quantitative analysis of signal amplitudes from TA and GS muscles for rats in different groups (intact, control, MN-EXO and MN-MSC). One-way ANOVA with Tukey's post hoc test for comparisons among multiple groups (*) and two-tailed paired t-tests were used for comparisons within groups (#) for the data shown in the violin plot. n = 18-41. ***p (or ###p) <

0.001, **p (or ##p) < 0.01, *p (or #p) < 0.05.